Available online at www.sciencedirect.com
ScienceDirect
Journal of Computational Physics 225 (2007) 1493–1507
JOURNAL OF COMPUTATIONAL PHYSICS
www.elsevier.com/locate/jcp

Conformal FDTD-methods to avoid time step reduction with and without cell enlargement

Igor Zagorodnov [a,*], Rolf Schuhmann [b], Thomas Weiland [c]

[a] DESY, Notkestrasse 85, 22603 Hamburg, Germany
[b] Universität Paderborn, EIM-E, Fachgebiet Theoretische Elektrotechnik, Warburger Strasse 100, 33098 Paderborn, Germany
[c] Technische Universität Darmstadt, Institut für Theorie Elektromagnetischer Felder, Schlossgartenstrasse 8, 64289 Darmstadt, Germany

Received 9 March 2006; received in revised form 31 January 2007; accepted 1 February 2007
Available online 16 February 2007

Abstract

During the last decades there have been considerable efforts to develop accurate and yet simple conformal methods for modelling curved boundaries within the finite difference time domain (FDTD) algorithm. In an earlier publication we proposed the uniformly stable conformal (USC) approach as a general three-dimensional extension of FDTD without the need to reduce the maximum stable time step. The main idea of USC is the usage of virtually enlarged cells near to the boundary, leading to an increased implementation effort. In this paper we review the USC method and introduce a new simple and accurate conformal scheme which does not use such enlarged cells. This simplified conformal (SC) scheme has the same number of operations and algorithmic logic as the standard "staircase" method, and thus is easily realizable in existing FDTD codes. Like USC, it leads to accurate results without time step reduction, showing a nearly second order convergence in practice. The method is verified and compared to other approaches by means of several numerical 2D and 3D examples.

Keywords: Maxwell's equations; FDTD; Finite integration; Conformal; Staircase; Wake field

1. Introduction

In the past decades, most of the research on FDTD [1] was focused on overcoming the staircase problem [2,3] of the conventional algorithm. These attempts have resulted in the development of various conformal versions of FDTD [4–16]. However, the most simple and accurate conformal methods (for example, [6,7]) demand to reduce the time step due to the reduction of the effective mesh step sizes near the boundary.

Several years ago, a new stable second order convergent algorithm on Cartesian grids *without time step reducing* was introduced in our paper [16]. The so-called uniform stable conformal (USC) algorithm was described in context of the finite integration technique [17–21] and is based on a conformal scheme introduced

* Corresponding author. Tel.: +49 40 8998 2755; fax: +49 40 8998 4305.
E-mail addresses: igor.zagorodnov@desy.de (I. Zagorodnov), schuhmann@tet.upb.de (R. Schuhmann), thomas.weiland@temf.de (T. Weiland).

0021-9991/$ - see front matter © 2007 Elsevier Inc. All rights reserved.
doi:10.1016/j.jcp.2007.02.002

in [6,7]. The main drawback of the USC algorithm is the usage of extended stencils near to the boundary (or, what is equivalent, exploiting of non-diagonal material matrices).

Motivated by the need for a simplification of USC, both in terms of implementation effort and intuitive understanding, we present in this paper a new simplified conformal (SC) scheme. It does not use extended stencils (or, what is equivalent, exploits only diagonal material matrices), but in the same time it remains accurate and stable without time step reducing. The new scheme is not second order convergent for general geometries. However, it is much more accurate than the "staircase" method. Numerical tests show a second order convergence of the new scheme on moderate meshes. Hence, as shows our experience, in practical examples the scheme has the same level of accuracy as the more complicated USC method. Like the USC scheme the new method is a fully three dimensional technique, with, however, a much simpler realization.

In the first section we shortly describe the finite integration technique (FIT) as the basis for our work, following the contents of the paper [21]. In the second part we review a powerful conformal method, the so-called partially filled cells (PFC) approach, which has been introduced as an extension of FIT in [7]. As an extension of PFC the USC method is reviewed and basic ideas are explained. The new simplified conformal scheme with diagonal material matrices and without time step reducing is introduced in the forth section. Finally, the convergence of the algorithm without the need to reduce the time step is analyzed on several numerical examples in two and three dimensions, and the method is compared with other approaches.

2. The finite integration technique

The conformal methods will be introduced in context of the finite integration technique [17–21].

We consider Maxwell's equations in their integral form on a domain $Q \subset R^3$,

$$\begin{aligned} &\oint_{\partial S} \vec{E}\cdot \mathrm{d}\vec{l} = -\frac{\mathrm{d}}{\mathrm{d}t}\int_S \vec{B}\cdot \mathrm{d}\vec{s}, \quad \oint_{\partial S} \vec{H}\cdot \mathrm{d}\vec{l} = \frac{\mathrm{d}}{\mathrm{d}t}\int_S \vec{D}\cdot \mathrm{d}\vec{s} + \int_S \vec{J}\cdot \mathrm{d}\vec{s}, \\ &\oint_{\partial V} \vec{D}\cdot \mathrm{d}\vec{s} = \int_V \rho\, \mathrm{d}v, \quad \oint_{\partial V} \vec{B}\cdot \mathrm{d}\vec{s} = 0, \end{aligned} \tag{1}$$

$(\forall S, V \subset Q)$, with linear, non-dispersive constitutive relations

$$\vec{D} = \varepsilon\vec{E}, \quad \vec{B} = \mu\vec{H}, \quad \vec{J} = \sigma\vec{E}, \quad (\forall x \in Q).$$

Let us start by introducing a grid-based decomposition of the entire computation domain into two dual cell complexes K and $\widetilde{K}$. We concentrate here on a three-dimensional Cartesian mesh, but the complete theory is also applicable to more general mesh types. Unlike in finite difference methods we do not start by allocating field components but rather by allocating the electric voltage along mesh edges and the magnetic flux through mesh cell facets as computational unknowns or state variables respectively:

$$\begin{aligned} &\widehat{e}_\vartheta = \int_{L_\vartheta} \vec{E}\cdot \mathrm{d}\vec{l}, \quad \widehat{h}_\vartheta = \int_{\widetilde{L}_\vartheta} \vec{H}\cdot \mathrm{d}\vec{l}, \\ &\widehat{\widehat{d}}_\vartheta = \int_{\widetilde{S}_\vartheta} \vec{D}\cdot \mathrm{d}\vec{s}, \quad \widehat{\widehat{b}}_\vartheta = \int_{S_\vartheta} \vec{B}\cdot \mathrm{d}\vec{s}, \quad \widehat{\widehat{j}}_\vartheta = \int_{\widetilde{S}_\vartheta} \vec{J}\cdot \mathrm{d}\vec{s}, \end{aligned}$$

where ϑ is a mesh multi-index, and $L_\vartheta, S_\vartheta \in K$, $\widetilde{L}_\vartheta, \widetilde{S}_\vartheta \in \widetilde{K}$ are the edges and facets of the primary and dual mesh, respectively. Solving the first Maxwell equation in integral form for the surface shown in Fig. 1(a) yields:

$$\widehat{e}_{xijk} + \widehat{e}_{yi+1jk} - \widehat{e}_{xij+1k} - \widehat{e}_{yijk} = -\frac{\mathrm{d}}{\mathrm{d}t}\widehat{\widehat{b}}_{zijk}.$$

with $i = 1..N_x, \quad j = 1..N_y, \quad k = 1..N_z$. Note, that this representation is still exact, as the $\widehat{e}_\vartheta$ are (by definition) the exact electric voltages along the edges of the surface, and similarly the $\widehat{\widehat{b}}_\vartheta$ represent the exact value of the magnetic flux density integral over the cell surface. (Note also the orientations in coordinate directions.)

If we compose column vectors $\widehat{\mathbf{e}}$ and $\widehat{\widehat{\mathbf{b}}}$ out of all voltage- and flux-components, we can write the combination of all equations over all surfaces in an elegant matrix form as

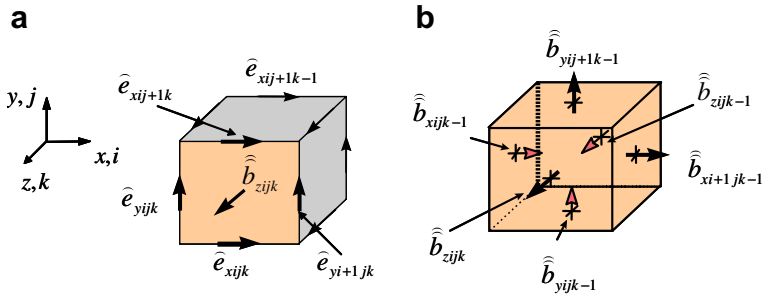

Fig. 1. Unit cell and state variables of the FIT.

$$\mathbf{C}\,\widehat{\mathbf{e}} = -\frac{\mathrm{d}}{\mathrm{d}t}\,\widehat{\widetilde{\mathbf{b}}}.$$

The matrix $\mathbf{C}$ picks the affected components out of the long vector to make up the corresponding equation. $\mathbf{C}$ is thus the discrete curl operator over the mesh K. On a $\{x, y, z\}$-coordinate grid with an appropriate indexing scheme the curl matrix has a 3×3 block structure:

$$\mathbf{C} = \begin{pmatrix} \mathbf{0} & -\mathbf{P}_z & \mathbf{P}_y \\ \mathbf{P}_z & \mathbf{0} & -\mathbf{P}_x \\ -\mathbf{P}_y & \mathbf{P}_x & \mathbf{0} \end{pmatrix}.$$

The two-banded, topological $\mathbf{P}_{\{x,y,z\}}$-matrices take the role of discrete partial differential-operators [20].

The second important differential operator in Maxwell's equations (1) is the div operator. In order to construct a discrete divergence operator we integrate Maxwell's equation $\oint_{\partial V} \vec{B} \cdot \mathrm{d}\vec{s} = 0$ over the entire surface of a mesh cell depicted in Fig. 1(b). From adding up the six relevant fluxes for each cell and by writing down all such equations for the entire cell complex we obtain a discrete analogue to the div-equation:

$$\mathbf{S}\,\widehat{\widetilde{\mathbf{b}}} = \mathbf{0}, \quad \mathbf{S} = (\,\mathbf{P}_x \quad \mathbf{P}_y \quad \mathbf{P}_z\,).$$

After an equivalent procedure for the remaining Maxwell equations by means of a dual mesh $\widetilde{K}$ we obtain a set of four discrete equations replacing Maxwell's equation on a grid doublet:

$$\mathbf{C}\,\widehat{\mathbf{e}} = -\frac{\mathrm{d}}{\mathrm{d}t}\,\widehat{\widetilde{\mathbf{b}}}, \quad \widetilde{\mathbf{C}}\,\widehat{\mathbf{h}} = \frac{\mathrm{d}}{\mathrm{d}t}\,\widehat{\widetilde{\mathbf{d}}} + \widehat{\widetilde{\mathbf{j}}}, \quad \mathbf{S}\,\widehat{\widetilde{\mathbf{b}}} = \mathbf{0}, \quad \widetilde{\mathbf{S}}\,\widehat{\widetilde{\mathbf{d}}} = \mathbf{q}. \tag{2}$$

They are completed by the discrete form of the material relations (constitutive equations) which appear (in the simplest linear case) as matrix equations

$$\widehat{\widetilde{\mathbf{d}}} = \mathbf{M}_\varepsilon\,\widehat{\mathbf{e}}, \quad \widehat{\widetilde{\mathbf{b}}} = \mathbf{M}_\mu\,\widehat{\mathbf{h}}, \quad \widehat{\widetilde{\mathbf{j}}} = \mathbf{M}_\sigma\,\widehat{\mathbf{e}}, \tag{3}$$

with the discrete permittivity matrix $\mathbf{M}_\varepsilon$, the permeability matrix $\mathbf{M}_\mu$, and the conductivity matrix $\mathbf{M}_\sigma$. Note that these material matrices contain both averaged material parameters and the lengths and areas of the grid edges and faces, respectively. In the case of orthogonal grid systems, including the Cartesian Yee-cell, all material operators can be defined as diagonal matrices (defining one-to-one relations between voltages and fluxes) and thus are trivially symmetric positive (semi)definite (s.p.d).

The complete set of Eqs. (2) and (3) is referred to as *Maxwell's Grid Equations* and the corresponding *discrete material equations*.

One of the most important properties, relating the base mesh curl operator $\mathbf{C}$ and the dual mesh *curl* operator $\tilde{\mathbf{C}}$, is the generalized symmetry

$$\tilde{\mathbf{C}} = \mathbf{C}^{\mathrm{T}}. \tag{4}$$

It follows directly from the duality of the pair of staggered meshes and can be easily proven by simple topological considerations. However, this property is of outstanding importance if these topological matrices are used as discrete curl-operators as in FIT, as we will show below.

From the topology of each the primary and the dual grid we have a second set of properties [20,21],

$$\mathbf{S}\mathbf{C} = \mathbf{0} \quad \text{and} \quad \widetilde{\mathbf{S}}\widetilde{\mathbf{C}} = 0, \tag{5}$$

which in the context of FIT can be interpreted as a discrete analogues to the vector-identity div curl = 0. Eq. (5) can be applied to prove many theorems concerning discrete electric and magnetic charges, as for example the discrete continuity equation.

Finally we can define a discrete grad operator with the properties

$$\mathbf{G} = -\widetilde{\mathbf{S}}^{\mathrm{T}} \quad \text{and} \quad \widetilde{\mathbf{G}} = -\mathbf{S}^{\mathrm{T}}. \tag{6}$$

From (5) and (6) we obtain $\mathbf{C}\mathbf{G} = \mathbf{0}$ and $\widetilde{\mathbf{C}}\widetilde{\mathbf{G}} = \mathbf{0}$, the discrete analogues to curl grad = 0. Eqs. (4)–(6) together with the symmetry of the material matrices build the foundation of basically all further properties of the discrete Maxwell equations as derived by the finite integration technique.

In the stability analysis we start with the *time-continuous* and *space-discrete* version of the discretization method (for the lossless case with $\mathbf{M}_\sigma = 0$):

$$\mathbf{C}\,\widehat{\mathbf{e}} = -\frac{\mathrm{d}}{\mathrm{d}t}\mathbf{M}_\mu\,\widehat{\mathbf{h}}, \quad \widetilde{\mathbf{C}}\,\widehat{\mathbf{h}} = \frac{\mathrm{d}}{\mathrm{d}t}\mathbf{M}_\varepsilon\,\widehat{\mathbf{e}}, \quad \rightarrow \quad \mathbf{M}_\varepsilon^{-1}\widetilde{\mathbf{C}}\mathbf{M}_\mu^{-1}\mathbf{C}\,\widehat{\mathbf{e}} = -\frac{\mathrm{d}^2}{\mathrm{d}t^2}\,\widehat{\mathbf{e}}\,. \tag{7}$$

Matrix $\mathbf{A} = \mathbf{M}_\varepsilon^{-1}\widetilde{\mathbf{C}}\mathbf{M}_\mu^{-1}\mathbf{C}$ is a product of two positive semidefinite matrices $\mathbf{A}_1 = \mathbf{M}_\varepsilon^{-1}$ and $\mathbf{A}_2 = \tilde{\mathbf{C}}\mathbf{M}_\mu^{-1}\mathbf{C}$. For arbitrary positive semidefinite matrices the following Lemma holds.

Lemma 1. *The product of two positive semidefinite matrices has only real and non-negative eigenvalues.*

For the case that one of the matrices is positive definite, the proof was given in [22, Theorem 7.6.3 and Theorem 1.3.20]. The result when both matrices are only positive semidefinite follows from the continuity of the eigenvalues on matrix entries.

It follows from Lemma 1 that all eigensolutions of the spatial discretization scheme expressed by this system matrix correspond to non-dissipative and non-growing oscillations with a real-valued circular frequency $\omega_i = \sqrt{\lambda_i}$ and the time-dependency $\widehat{\mathbf{e}}(t) \propto Re\{\mathrm{e}^{\mathrm{j}\omega_i t}\}$. This is the proof for the *space stability* of the time-continuous formulation of the Maxwell's Grid equations.

The next step in the stability analysis for the complete time domain algorithm is the stability of the time-stepping scheme applied to this system. Discretization of (7) in time using the leap-frog scheme leads to

$$\widehat{\mathbf{h}}^{n+1} - \widehat{\mathbf{h}}^{\,n} = -\Delta t\mathbf{M}_\mu^{-1}\mathbf{C}\widehat{\mathbf{e}}^{n+\frac{1}{2}}, \quad \widehat{\mathbf{e}}^{n+\frac{3}{2}} - \widehat{\mathbf{e}}^{n+\frac{1}{2}} = \Delta t\mathbf{M}_\varepsilon^{-1}\widetilde{\mathbf{C}}\widehat{\mathbf{h}}^{n+1},$$

which after resolving the curl matrices is *computationally equivalent* to the common FDTD update equations (at least for the standard case considered so far). A necessary and sufficient condition for *time stability* is the *generalized Courant-criterion* [21]

$$|\Delta t\omega_{\mathbf{A}}| \leqslant 2 \rightarrow \Delta t \leqslant \Delta t_{\max} = \frac{2}{\max|\omega_{\mathbf{A}}|}. \tag{8}$$

It describes *exactly* the stability-limit for uniform as well as non-equidistant (or even non-Cartesian) meshes with inhomogeneous material distributions. For the simplest case (homogeneous permittivity ε and permeability μ and constant mesh step sizes $\Delta x, \Delta y, \Delta z$) it reduces to the well-known formula

$$\Delta t \leqslant \Delta t_C = \sqrt{\frac{\varepsilon\mu}{L_x^{-2} + L_y^{-2} + L_z^{-2}}}. \tag{9}$$

Recently, the commonly used generalization of (9) for non-uniform Cartesian meshes and non-homogenous domains,

$$\Delta t \leqslant \Delta t_C = \min_i \sqrt{\frac{\varepsilon_i \mu_i}{L_{x,i}^{-2} + L_{y,i}^{-2} + L_{z,i}^{-2}}}, \tag{10}$$

was proven [23], where minimization is over all primary cells.

3. Review of conformal schemes

3.1. Partially filled cells (PFC) approach

With a standard staircase approximation of curved boundaries we obtain only a first order convergent scheme in the L_2^h grid norm. To improve the convergence, in this section we review in this section the partially filled cells (PFC) approach for perfectly conducting (PEC) geometries, resulting in a second order convergent scheme. This scheme is fully equivalent to the schemes presented in [6,7]. In the following we consider only the case of the constant scalar material parameters ε, μ in the domain Q.

In the standard staircase approximation, the elements of the diagonal $\mathbf{M}_\varepsilon$ and $\mathbf{M}_\mu$ matrices are (without double indices for simplicity of notation)

$$\hat{\varepsilon}_{pijk} = \varepsilon \frac{\widetilde{S}_{pijk}}{L_{pijk}}, \quad \hat{\mu}_{pijk} = \mu \frac{S_{pijk}}{\widetilde{L}_{pijk}} \tag{11}$$

with $p = x, y, z$ and the face areas and edge lengths of the primary and secondary mesh $S, L, \widetilde{S}, \widetilde{L}$, respectively.

To derive a conformal scheme, we allow the cells of the computational grid to be only partially filled by a PEC material (thus partially filled cells-approach, PFC) with an arbitrarily shaped interface. To model this case we will modify only the elements of the material matrices:

$$\hat{\varepsilon}_{pijk} = \varepsilon \frac{\widetilde{S}_{pijk}}{l_{pijk}}, \quad \hat{\mu}_{pijk} = \mu \frac{s_{pijk}}{\widetilde{L}_{pijk}}, \tag{12}$$

where s, l denote reduced cell facet areas and edge lengths, including only those parts inside the computational domain (outside PEC material), as shown in Fig. 3a. This modification follows intuitively from the integral nature of the FIT approach, and the second order convergence of this scheme was proven in [16].

Next we will consider the stability of this extended scheme. Obviously, the extended matrices from (12) are still s.p.d., and the system is *spatially stable*. To analyze the *time stability* and to obtain the limit for the maximum stable time step, we express the inverse material matrices $\mathbf{M}_{\varepsilon^{-1}}$, $\mathbf{M}_{\mu^{-1}}$ by a composition of diagonal matrices

$$\mathbf{M}_{\varepsilon^{-1}} = \varepsilon^{-1} \overline{\mathbf{L}} \mathbf{R}, \quad \mathbf{M}_{\mu^{-1}} = \mu^{-1} \overline{\mathbf{S}}^{-1} \widetilde{\mathbf{R}}, \tag{13}$$

with elements

$$\bar{l}_{pijk} = \frac{l_{pijk}}{L_{pijk}}, \quad \bar{s}_{pijk} = \frac{s_{pijk}}{S_{pijk}}, \quad r_{pijk} = \frac{L_{pijk}}{\widetilde{S}_{pijk}}, \quad \tilde{r}_{pijk} = \frac{\widetilde{L}_{pijk}}{S_{pijk}}. \tag{14}$$

$\mathbf{R}$ and $\widetilde{\mathbf{R}}$ contain the metrics of the grid and transform flux into voltage quantities. The entries of $\varepsilon^{-1}\overline{\mathbf{L}}$ and $\mu^{-1}\overline{\mathbf{S}}^{-1}$ describe some kind of effective (inverse) material parameters, scaled by the ratio of the non-PEC part of the corresponding edge or face. Compared to the staircase model, they take the role of the undisturbed material values in the Courant criterion (10). However, we may now have $\mu_\vartheta \ll \mu$ in boundary cells, if the non-PEC part of the area is very small ($s_\vartheta \ll S_\vartheta$), and thus the time step has to be reduced. As follows from [23], a sufficient condition for the numerical stability of the algorithm is

$$\Delta t \leqslant \min \sqrt{\frac{\varepsilon_\gamma \mu_\theta}{L_x^{-2} + L_y^{-2} + L_z^{-2}}}, \tag{15}$$

where the multi-index γ is defined such, that γ corresponds to the boundary edges of face S_θ.

In order to limit the reduction of the time step to reasonable values, cells with a PEC part larger than 99% are usually replaced by completely filled ones (introducing a small approximation error). This leads with (15) to the estimation

$$\Delta t \leqslant 0.1\Delta t_C. \tag{16}$$

Numerical experience (cf. also the examples below) shows, that this stability limit is a very strong condition. The *exact* stability limit can be obtained (also in practice) by the maximum eigenvalue of the curl–curl system matrix of the PFC model and (8).

3.2. Uniformly stable conformal (USC) scheme

In this section we review the USC algorithm [16] and explain its basic idea to overcome the main drawback of the PFC method: the time step reduction compared to the conventional "staircase" method.

As a simple example we consider the one-dimensional (1D) problem in Fig. 2a:

$$\mu\frac{\partial H}{\partial t} = \frac{\partial E}{\partial z}, \quad \varepsilon\frac{\partial E}{\partial t} = \frac{\partial H}{\partial z}, \quad E(0) = E(1) = 0. \tag{17}$$

Let the factor $s \in [0, L]$ (where L is the uniform mesh step) describe the size of the last mesh cell facet. Fig. 2(b) shows the dependence of the maximal stable normalized time step $\Delta\tau = c\Delta t$ from the cell facet area reduction factor $\bar{s} = s/L$. The mesh is composed by $n = 100$ cells. As can be seen, a sufficient condition to avoid time step reduction for 1D case has the form

$$\bar{s} \geqslant 0.5. \tag{18}$$

The simplest way to avoid the time step reduction in 1D is to merge together cell facets n and $n-1$ (see Fig. 2a) if condition (18) violated. But as it was shown in [5,11] a generalization of this idea on 2D and 3D case is quite complicated.

In our numerical experiments we have found that the sufficient condition (18) (to avoid time step reduction for 2D and 3D cases) can be refined as

$$\bar{s}_\theta \geqslant 0.5\bar{l}_\gamma. \tag{19}$$

(with multi-indices γ, θ and notations as above, see also Fig. 3a).

Hence, for cells whose parameters do not fulfill condition (19) a special treatment is required as will be described in this and the next sections. First, we consider the quite complicated USC approach which preserves the second order convergence of the original PFC scheme. Later, in Section 4, we will describe a very simple but still efficient new method.

Consider Fig. 3a. To calculate the flux $\widehat{b}_{zijk}$ through the reduced face s_{zijk} in the PFC scheme described above we use only the non-zero voltages $\widehat{e}_{yi+1jk}$ and $\widehat{e}_{xijk}$ along the reduced edges l_{yi+1jk} and l_{xijk}. Appar-

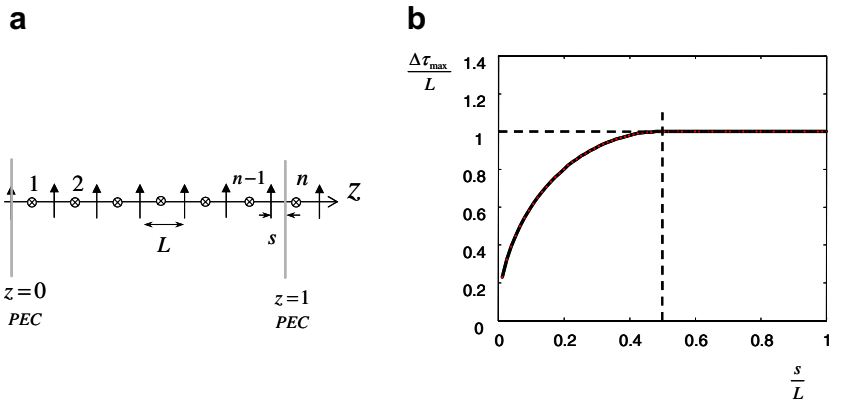

Fig. 2. The time step reduction in 1D.

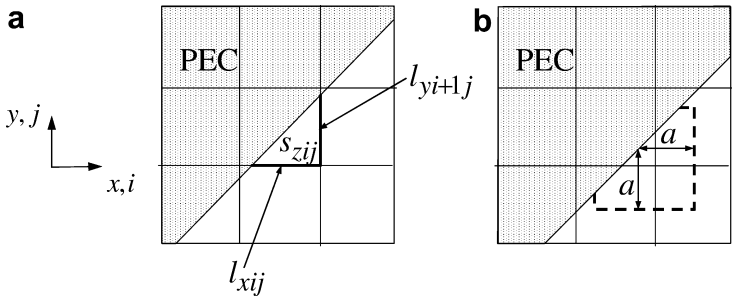

Fig. 3. Curved PEC-boundary in a Cartesian mesh (z-slice with index k).

ently, this information is not sufficient to do the same "big" time step in this small cell, which we can use for cells inside the calculation domain. The idea of the USC method is to use also the information from the adjacent cells to enlarge the local curl-operation and thus to enable the usage of the same time step as before.

To this end, we will build an approximation of the virtual cell facet shown by the dashed line in Fig. 3(b) *for boundary cells only*. This means, that inside the domain we can still use the conventional FIT algorithm. The update equations of the electric components will not be changed at all compared to the PFC scheme.

To ease the stability analysis, all modifications are realized formally by adding some non-diagonal elements in the material matrix $\mathbf{M}_{\mu^{-1}}$, leaving the topological curl matrix $\mathbf{C}$ untouched. That means, instead of interpolating electric voltages to perform directly an extended curl-operation, we follow a slightly different idea: After calculating all adjacent magnetic fluxes in a regular way, they are interpolated to find the magnetic voltage. However, it will be shown below for a simple example, that this can also be geometrically interpreted as an enlarged curl-operations. Again we restrict the derivation to homogeneous domains with constant material parameters μ, ε. A generalization to the non-homogenous case is straightforward.

The new material matrix $\widetilde{\mathbf{M}}_{\mu^{-1}}$ is composed by the relation

$$\widetilde{\mathbf{M}}_{\mu^{-1}} = \mu^{-1}\mathbf{V}^{*}\mathbf{D}\mathbf{V}, \tag{20}$$

where the diagonal matrix $\mathbf{D}$ is responsible for the order of the approximation, and $\mathbf{V}$ is a matrix of weights. As can be seen below, already the representation $\widetilde{\mathbf{M}}_{\mu^{-1}} \sim \mu^{-1}\mathbf{D}\mathbf{V}$ would result in a second order convergent scheme with enlarged cell facets. Such a non-symmetric material matrix, however, would violate the spatial stability of the scheme and lead to late time instabilities. Thus, the symmetrized representation with the transposed matrix $\mathbf{V}^{*}$ has to be preferred.

To simplify the notation, we consider only one plane parallel to the xy-plane and omit the index k for the z-direction. First we build an auxiliary matrix $\mathbf{V}^0$ (the small symbols demonstrate the operator stencil) with

$$\begin{aligned}
&v^0_{zij,zij} = 1(\boxplus);\\
&v^0_{zij,zi+1j} = \max(0, a - \bar{s}_{zij}\bar{l}^{-1}_{yi+1j})(\boxplus);\ v^0_{zij,zi-1j} = \max(0, a - \bar{s}_{zij}\bar{l}^{-1}_{yij})(\boxplus);\\
&v^0_{zij,zij+1} = \max(0, a - \bar{s}_{zij,zij}\bar{l}^{-1}_{xij+1})(\boxplus);\ v^0_{zij,zij-1} = \max(0, a - \bar{s}_{zij}\bar{l}^{-1}_{xij})(\boxplus);
\end{aligned} \tag{21a}$$

and

$$\begin{aligned}
&v^0_{zij,zi+1j+1} = v^0_{zij,zi+1j}v^0_{zij,zij+1}(\boxplus);\ v^0_{zij,zi-1j+1} = v^0_{zij,zi-1j}v^0_{zij,zij+1}(\boxplus);\\
&v^0_{zij,zi+1j-1} = v^0_{zij,zi+1j}v^0_{zij,zij-1}(\boxplus);\ v^0_{zij,zi-1j-1} = v^0_{zij,zi-1j}v^0_{zij,zij-1}(\boxplus).
\end{aligned} \tag{21b}$$

Here, $a \in [0.5, 1)$ is a constant parameter. In all numerical examples shown in the next section a was taken equal to 0.5 (in accordance with condition (19)). As a consequence, only those cell facets are considered in the construction of the matrix $\mathbf{V}^0$ which are filled more than 50% by a PEC material. From the relations above we can also see that only cells near the boundary will give a contribution to non-diagonal elements of the matrix $\mathbf{V}^0$.

From the matrix $\mathbf{V}^0$ we will build a normalized matrix $\mathbf{V}$:

$$v_{zij,zi_1j_1} = v^0_{zij,zi_1j_1} \Big/ \sum\nolimits_{i_2j_2} v^0_{zi_2j_2,zi_1j_1}, \tag{22}$$

where the summa is taken over all elements of corresponding column. Why do we need this normalization? The matrix $\mathbf{V}^*$ should not spoil the already available approximation. The relation (22) means that the sum of all elements of any row of matrix $\mathbf{V}^*$ is equal to 1. Hence multiplication by matrix $\mathbf{V}^*$ is equivalent to some averaging and the local approximation error in the boundary cells remains of the first order.

Finally we build the diagonal matrix $\mathbf{D} = \widetilde{\mathbf{L}}\mathbf{U} > 0$ with $\widetilde{\mathbf{L}} = \|\widetilde{L}_{pijk}\|$ and a diagonal matrix $\mathbf{U}$ with elements

$$u_{zij} = \left(\sum_{i_1j_1} v_{zij,zi_1j_1} s_{zi_1j_1} \right)^{-1}, \tag{23}$$

where the summa is taken over all elements of the corresponding row.

Relations (22) and (23) allow us to show that we have an at least first order local approximation error in the material relations in the boundary cells. Globally this ensures a second order convergent scheme in the L_2^h grid norm if it is stable [16].

For spatial stability, it follows directly from construction of the material matrix $\widetilde{\mathbf{M}}_{\mu^{-1}}$ that the system matrix $\mathbf{A} = \widetilde{\mathbf{M}}_{\mu^{-1}}\mathbf{C}\mathbf{M}_{\varepsilon^{-1}}\mathbf{C}^{\mathrm{T}}$ has only real non-negative eigenvalues.

A limit for the maximum stable time step (defining the time stability of the method) can not be found by an analytical proof. However, the numerical examples in the next section show that the time step has not to be reduced in all cases which have been tested (including many cases with odd geometries, e.g. sharp corners).

Above, all relations were given for one coordinate plane and constant index k. For other coordinate planes we have the same relations which are not coupled with the relations for orthogonal planes.

3.3. Geometric interpretation of USC scheme

The new material matrix $\widetilde{\mathbf{M}}_{\mu^{-1}} = \mu^{-1}\mathbf{V}^*\mathbf{D}\mathbf{V}$ is non-diagonal, and is composed as a product of three matrices. The entries of the matrix $\mathbf{V}$ represent the interpolation of magnetic flux contributions from neighbouring cells. For example, the coefficient $v_{zijk,i+1jk}$ has the meaning of the contribution of the magnetic flux through the z-facet $i+1, j, k$ to the magnetic flux through the z-facet i, j, k. The entries of the diagonal matrix $\mathbf{D}$ represent the inverse areas of the enlarged interpolated facets. Hence, the matrix $\mathbf{D}$ converts the interpolated fluxes in voltages. Finally, the matrix $\mathbf{V}^*$ is the transposed matrix of $\mathbf{V}$ and averages the neighbouring magnetic voltages. We do need to include the matrix $\mathbf{V}^*$ here in order to obtain a symmetric matrix $\widetilde{\mathbf{M}}_{\mu^{-1}}$ which ensures the late-time stability of the scheme.

For a geometric interpretation of the weights defined by the USC procedure we first consider the simple case in Fig. 4a, where the interface to the PEC material is parallel to the yz-coordinate plane, with a vacuum to PEC-ratio of $\beta < a$. This leads to

$$\bar{s}_{zij} = \bar{l}_{xij} = \bar{l}_{xij+1} = \beta, \quad \bar{l}_{yi+1j} = \bar{l}_{yi+2j} = \bar{l}_{xi+1j} = \bar{l}_{xi+1j+1} = 1,$$

and all entries of the corresponding row of $\mathbf{V}^0$ are zero except for $v^0_{zij,zi+1j} = a - \beta$. From (22) and (23) we obtain

$$v_{zij,zi+1j} = \frac{a-\beta}{1+a-\beta}, \quad v_{zij,zij} = 1, \quad u_{zij} = \frac{1}{s_{zij} + s_{zij,zi+1j} v_{zij,zi+1j}}.$$

Returning to Fig. 4a, and remembering that each of the magnetic flux-components involved is calculated by a local curl of electric voltages, we can now see, that this weighting procedure is indeed equivalent to a local curl around the virtual cell facet with step size u^{-1}_{zij} using interpolated electric voltages. Finally the obtained flux is correlated with the enlarged area of this virtual cell facet to be transformed into a magnetic voltage.

A similar, but more complicated geometric interpretation is possible also for the general case (of arbitrarily shaped interface planes) shown in Fig. 4(b). It is adapted from the paper [24], where the authors propose a so-called *enlarged cell technique* (ECT) with the same objective as for the USC method (see also [28,29]). The derivation of ECT uses a somehow mixed FIT-FDTD notation with "electromotive forces", which are equivalent to the electric voltages here. Although magnetic fluxes are not explicitly defined, a closer look reveals that

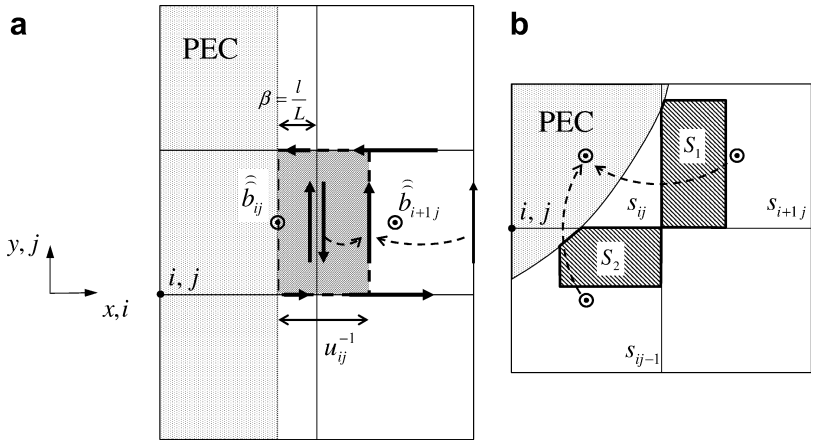

Fig. 4. Geometric interpretation of weighting procedure: (a) parallel interface and (b) general interface (adapted from Fig. 1b in [24], with notations of this paper).

(exactly like in USC) these magnetic fluxes are the quantities which are averaged to handle the virtually enlarged cells. The main idea is that the weighting of adjacent cell information is controlled by the size of the areas intruding the neighbouring cells (cf. Fig. 4(b) and [24] for the formulas in detail.) As we show in the Appendix, it turns out that at least for this (still not completely general) example ECT and USC coincide. It should be noted, however, that USC is more general in the sense that it defines unique formulas for arbitrary cases (whereas in ECT one has to decide in which direction cells should be enlarged in order to avoid the case of simultaneously "intruding" and "intruded" cells). Even more important, the strict FIT notation used for USC has the advantage to give a strict proof for spatial stability, whereas the demand for symmetric interpolation operators is not so clearly motivated in the formulas in [24].

4. Simplified conformal (SC) scheme to avoid time step reduction with diagonal material matrices

The USC technique described so far is a second order convergent algorithm without time step reduction. However, if we relax our demand on the order of convergence, a very simple conformal method can be obtained which in most cases shows an accuracy compared with the USC algorithm. In any case its accuracy is approximately one order of magnitude better as that of the "staircase" method.

In the USC method we have enlarged the cells whose parameters do not fulfill the geometric condition (19). But another and more direct way to proceed is to change the mesh parameters in such way that condition (19) holds everywhere. What has to be changed? Areas or lengths l_γ? Or both? From an intuitive point of view the change of lengths is a smaller distortion of the mesh than change of areas. It will be confirmed in the numerical tests in the last section.

The easiest way to insure validity of condition (19) is to completely avoid the area reduction of the cell facets. Only the edge length reducing is allowed. It means that we assign $\bar{s}_\theta = 1$ for all cell facets which are not completely located in PEC material, but l_γ coefficients are calculated accurately. This method in FDTD notation was described by Yu and Mittra in [12], but as was shown by us in [16] it may behave even worse than an "optimal" (in the sense of a best possible) staircasing.

Next we consider more accurate modification of cell facets areas in accordance with the law

$$\bar{s}_\theta = \max(0.5 \max(\bar{l}_\gamma), \bar{s}_\theta), \tag{24}$$

where the multi-index γ corresponds to the 4 boundary edges of face S_θ. It is easy to see that after the modification (24) the condition (19) holds and the USC method is not required. In a practical realization we should first discretize the geometry and find the reduced facet areas s_θ and edge lengths l_γ of the primary mesh cells near the PEC boundary. Then the areas are modified in accordance with (24). Hence this method only modifies the material matrix $\mathbf{M}_{\mu^{-1}}$ of the PFC algorithm, but leaves it diagonal. We will call this approach s-method.

A much more effective and accurate way is to leave the material matrix $\mathbf{M}_{\mu^{-1}}$ as it is in the PFC algorithm and to modify only the matrix $\mathbf{M}_{\varepsilon^{-1}}$ in accordance with the modification of edge lengths by the law

$$\bar{l}_\gamma = \min(2\min_\theta(\bar{s}_\theta), \bar{l}_\gamma), \tag{25}$$

where the multi-indexes θ correspond to 4 faces adjacent to boundary edge l_γ. In the index notation relation (25) can be rewritten as (see Fig. 1)

$$\begin{aligned}
\bar{l}_{xijk} &= \min(2\min(\bar{s}_{yijk}, \bar{s}_{yij(k-1)}, \bar{s}_{zijk}, \bar{s}_{zi(j-1)k}), \bar{l}_{xijk}),\\
\bar{l}_{yijk} &= \min(2\min(\bar{s}_{xijk}, \bar{s}_{xij(k-1)}, \bar{s}_{zijk}, \bar{s}_{z(i-1)jk}), \bar{l}_{yijk}),\\
\bar{l}_{zijk} &= \min(2\min(\bar{s}_{xijk}, \bar{s}_{xi(j-1)k}, \bar{s}_{yijk}, \bar{s}_{y(i-1)jk}), \bar{l}_{zijk}).
\end{aligned} \tag{26}$$

Again it is easy to see that after the modification (25) condition (19) holds and the USC method is not required. This method modifies only the material matrix $\mathbf{M}_{\varepsilon^{-1}}$ of the PFC algorithm, but leaves it diagonal. We will call this approach simplified conformal (SC) method, and it will be shown by the numerical examples in the next section that it is much more accurate than the s-method (24).

5. Numerical examples

In this section we present some 2D and 3D examples calculated with the described schemes.

To check the convergence of the USC and SC schemes without reduction of the time step we start with three two-dimensional numerical examples: resonant oscillations in a square, a circle and a ring. In all validation examples we set an initial field in the entire calculation domain corresponding to an analytically determined eigensolution [25] and start the time stepping-procedure. After a (long enough) period of time T we compare the numerical solution with the exact one. For simplicity we use a series of equidistant meshes with the step sizes $L_x = L_y = L$ and free space with $c = (\varepsilon_0\mu_0)^{-\frac{1}{2}}$.

Our first example is a perfectly conducting circle. The magnetic field of the TE mode

$$H_z(\rho, \theta, t) = -J_1(k\rho)\cos(\theta)\sin(kct), \quad ka = 8.5363, \quad a = \frac{d}{2},$$

is compared to the numerical solution after a period of time $T = c^{-1}d/\sqrt{2}$, where d is the diameter of the circle. The relative error of the numerical solution $\widetilde{H}_z$

$$\delta = \frac{\|H_z - \widetilde{H}_z\|_{L_2^h}}{\|H_z\|_{L_2^h}} \tag{27}$$

is shown in Fig. 5a by a solid black line for the USC scheme. The grey line shows results for the new SC scheme. The convergence of the PFC scheme is shown by a line with circles, and for the staircase approxima-

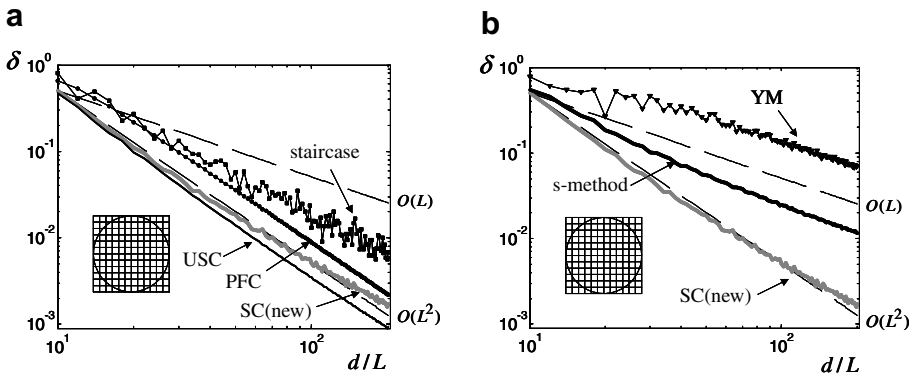

Fig. 5. Convergence of different methods for circle.

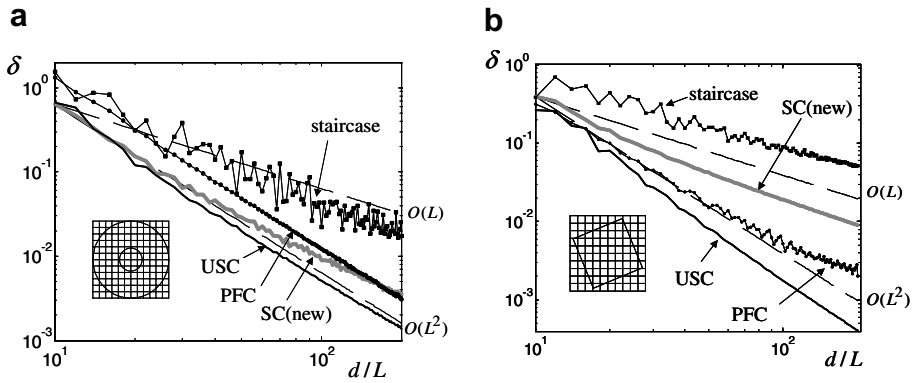

Fig. 6. Convergence of different methods for ring (a) and square (b).

tion it is shown by line with squares. In this and next tests all schemes except the PFC method are taken with maximal stable time step of the staircase scheme. For the PFC method we have excluded the cell facets with an area less then 1% and used three times smaller time step. As we can see the new SC scheme shows very accurate results and an almost second order convergence.

In Fig. 5(b) we have analyzed the s-method and the Yu–Mittra (YM) approach [12]. It is easy to see that the s-method behaves worse than the SC scheme. It is even more interesting to see that the results of the s-method and of YM are worse than the "optimal" (best possible) staircase method, where we have excluded cell facets filled with PEC material more than by 50% and have expanded all other cell facets.

Fig. 6a shows the data for the ring, and the TE mode

$$H_z(\rho,\theta,t) = -\left(J_1(k\rho) - \frac{J_1'(ka)}{N_1'(ka)}N_1(k\rho)\right)\cos(\theta)\sin(kct),$$

$$ka = 9.308266, \quad a = \frac{10}{3}, \quad b = \frac{d}{2},$$

where a is an exterior and b is an interior radius of the ring. Again, the new SC scheme shows almost a second order convergence.

Finally, Fig. 6(b) shows the most stringent test: a perfectly conducting square rotated by the angle $\pi/8$ relative to the x-axis. The magnetic field of the TE mode (for the non-rotated case),

$$H_z(x,y,t) = -\cos\left(\frac{x+a}{\sqrt{2}}k\right)\cos\left(\frac{y+a}{\sqrt{2}}k\right)\sin(kct), \quad ka = \sqrt{2}\pi, \quad a = \frac{d}{2\sqrt{2}},$$

is rotated by the angle $\pi/8$ and compared to the numerical solution after a period of time $T = c^{-1}d/\sqrt{2}$, where d is the diagonal of the square. Here, the SC scheme shows a first order convergence. However, the accuracy of the scheme is one order of magnitude better as obtained with the staircase approach.

In all examples the USC scheme as expected shows second order convergence. The new SC scheme shows an accuracy comparable with the USC scheme and is at least by one order of magnitude better than the conventional "staircase" scheme (in its "optimal" application). Note that the new simplified conformal scheme shows a second order convergence in all examples considered in [24].

In the next test we slightly change the analysis procedure and perform an eigenvalue analysis of a sphere (3D) and a cylinder (quasi-2D, as above) in frequency domain, rather than actually doing the time stepping. This allows to see directly the accuracy of the spatial discretization by the PFC and SC schemes as a function of the mesh step sizes. We use again an equidistant discretization for a quarter of the structures (for symmetry reasons) and compare the numerical eigensolutions of the first TM modes with their analytical values. The results in Fig. 7 show that SC performs better than the s-method, and in the quasi-2D example as well as the underlying PFC scheme. In the fully 3D example the accuracy of SC does not reach the PFC results, but we still have a smooth convergence curve, far below the staircase results.

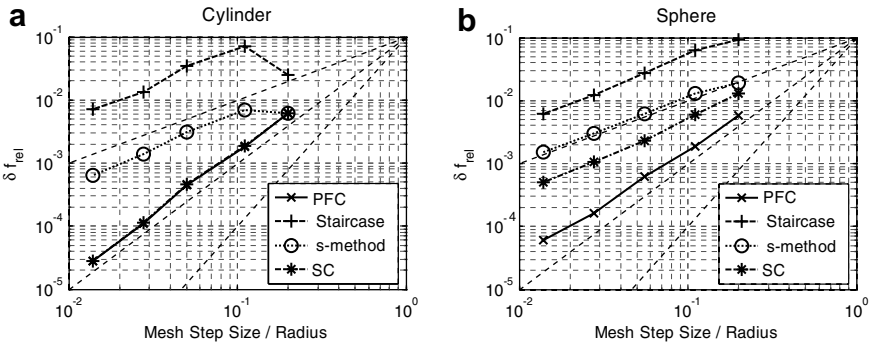

Fig. 7. Convergence of the SC scheme and the s-method versus the PFC scheme: Eigenvalue analysis of the first TM eigenmodes in a cylinder (quasi-2D) and a sphere (fully 3D) for varying mesh step sizes.

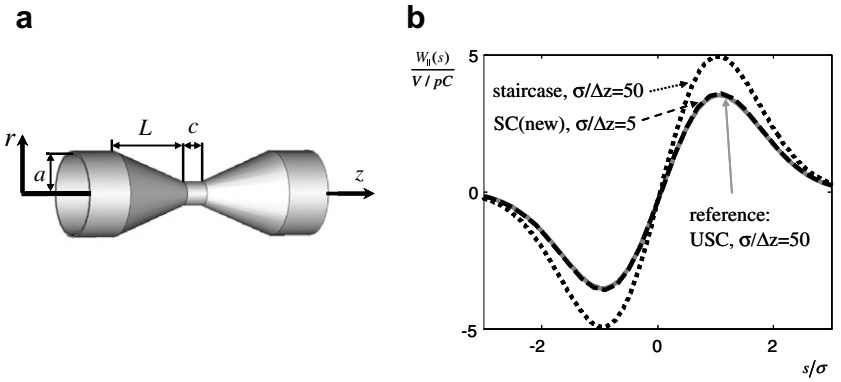

Fig. 8. Longitudinal wake potential of tapered rotationally symmetric collimator.

As a further test example we use the circular collimator structure shown in Fig. 8a (with inner radius b not indicated in the figure). More details and definition of the wake potential can be found in [26]. In this example we use the SC method in combination with a semi-implicit scheme that allows to leave the longitudinal edges of the mesh as accurate as in PFC scheme and to restrict the modification (25) only to edges in the transverse plane. Fig. 8(b) shows the results for the monopole wake field of the relativistic Gaussian bunch moving on the axis, comparing the result of the staircase scheme to the one obtained with the new SC scheme. The geometric parameters are $a = 10$ mm, $L = 400$ mm and $c = 20$ mm, $b = 1$ mm, where b is the inner radius of the collimator. Already with a coarse resolution of only 5 mesh points per bunch length $\sigma = 0.5$ mm the new SC scheme gives much more accurate result than the staircase scheme with a 10 times denser mesh.

Finally, we test the SC scheme on the example of a three dimensional rectangular collimator shown in Fig. 9a (with inner aperture $b \times a$, b is not indicated in the figure). Again, we use the SC method with semi-implicit scheme [27] that allows to leave the longitudinal edges of the mesh as accurate as in PFC scheme and to restrict modification (25) only to edges in transverse plane as follows:

$$\bar{l}_{zijk} = \bar{l}_{zijk}, \quad \bar{l}_{yijk} = \min(2\min(\bar{s}_{xijk}, \bar{s}_{xij(k-1)}), \bar{l}_{yijk}), \quad \bar{l}_{xijk} = \min(2\min(\bar{s}_{yijk}, \bar{s}_{yij(k-1)}), \bar{l}_{xijk}).$$

Fig. 9(b) shows the results for the monopole wake field of the relativistic Gaussian bunch moving on the axis. It compares the result of the staircase scheme to the one obtained with the new SC scheme. The geometric parameters ($a = 38$ mm, $L = 103.8$ mm and $c = 0.4$ mm, $b = 1.4$ mm, where b is the height of the collimator aperture) describe one of the collimators planned for future experiments in Stanford Linear Accelerator Center [30]. With 5 points per bunch length $\sigma = 1$ mm the new SC scheme gives much more accurate result than the staircase scheme.

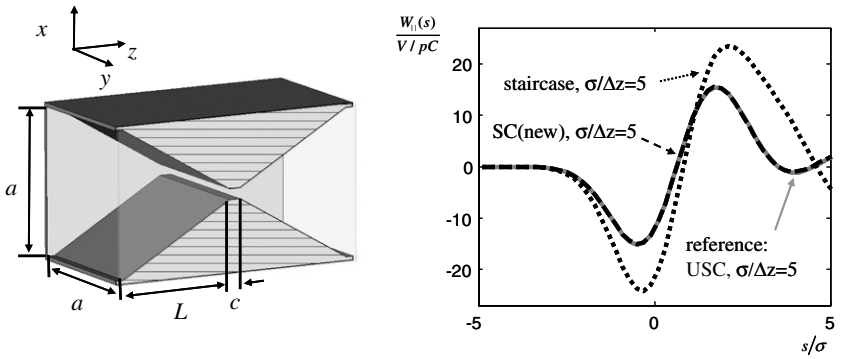

Fig. 9. Longitudinal wake potential of tapered rectangular collimator.

6. Conclusion

We have developed two conformal FIT/FDTD-schemes which are capable to model curved PEC boundaries in a Cartesian mesh without the need to reduce the maximum stable time step. The more complicated USC scheme uses information of adjacent cells, leading to an extended operator stencil for some cells at the boundary with an increased implementation effort. However, it shows the full second order accuracy of the underlying PFC approach. On the other hand, the new simplified conformal (SC) scheme differs from the conventional staircase scheme only by a simple modification of some coefficients. Thus, it is computationally as efficient as the standard method and the implementation effort is very low. Their derivation being based on the FIT methodology, both algorithms can be interpreted geometrically and have strict proofs for the spatial stability.

The numerical validation of the algorithms by means of several numerical 2 D and 3D geometries, including an application from accelerator technology, shows that USC and SC are numerically stable *without reducing the time step*. Compared to the PFC method the USC and SC approaches show comparable levels of accuracy, but are faster than PFC at least by a factor of 3.

The schemes are fully three dimensional and their implementation in general simulation codes are straightforward. Beyond their application in a standard FDTD code they have been successfully used in combination with a semi-implicit time integration method for large-scale wake field computations.

Appendix. Coefficients in the ECT scheme

Referring to Fig. 4(b), the interpolation coefficients of the ECT scheme (Fig. 1b and Eqs. (6)–(13) in [24]) can be translated into the FIT notation. Since the update equations for the electric field components are not changed in both USC and ECT, we consider only the update equation for the magnetic field components, which in FIT notation reads

$$\widehat{\mathbf{h}}^{n+1} = \widehat{\mathbf{h}}^{n} - \Delta t \widetilde{\mathbf{M}}_{\mu^{-1}} \mathbf{C} \widehat{\mathbf{e}}^{n+0.5}.$$

We decompose the material matrix as $\widetilde{\mathbf{M}}_{\mu^{-1}} = \widetilde{\mathbf{L}} \widehat{\mathbf{M}}_{\mu^{-1}}$ (extracting the dual edge lengths) and will show that the matrix $\widehat{\mathbf{M}}_{\mu^{-1}}$ is the same in both variants. From [24] it is easy to check that the ECT description result in a matrix (only three rows and columns are shown, referring to components $(i+1jk)$, (ijk) and $(ij-1k)$)

$$\widehat{\mathbf{M}}_{\mu^{-1}} = \frac{1}{\mu} \begin{Vmatrix} \frac{1}{s_{i+1j}} \left(1 + N_1 \left(\frac{s_1}{S_{\text{stab}}} - 1\right)\right) & \frac{1}{S_{\text{stab}}} N_1 & \frac{1}{S_{\text{stab}}} N_1 N_2 \\ \frac{1}{S_{\text{stab}}} N_1 & \frac{1}{S_{\text{stab}}} & \frac{1}{S_{\text{stab}}} N_2 \\ \frac{1}{S_{\text{stab}}} N_1 N_2 & \frac{1}{S_{\text{stab}}} N_2 & \frac{1}{s_{ij-1}} \left(1 + N_2 \left(\frac{s_2}{S_{\text{stab}}} - 1\right)\right) \end{Vmatrix}, \tag{A.1}$$

where

$$N_1 = \frac{S_1}{s_{i+1j}}, \quad N_2 = \frac{S_2}{s_{ij-1}}, \quad S_{\text{stab}} = s_{ij} + S_1 + S_2.$$

Note that the reduced cell facets are denoted with capital letters and index 'xy' in [24]. Now we follow the USC approach as described above and build the matrix

$$\mathbf{V}^0 = \begin{Vmatrix} 1 & 0 & 0 \\ v_1^0 & 1 & v_2^0 \\ 0 & 0 & 1 \end{Vmatrix}, \quad v_1^0 \equiv v^0_{ij,i+1j}, \quad v_2^0 \equiv v^0_{ij,ij-1}.$$

From the averaging procedure (22) we obtain

$$\mathbf{V} = \begin{Vmatrix} 1-v_1 & 0 & 0 \\ v_1 & 1 & v_2 \\ 0 & 0 & 1-v_2 \end{Vmatrix} = \begin{Vmatrix} \frac{1}{1+v_1^0} & 0 & 0 \\ \frac{v_1^0}{1+v_1^0} & 1 & \frac{v_2^0}{1+v_2^0} \\ 0 & 0 & \frac{1}{1+v_2^0} \end{Vmatrix}.$$

Matrix $\mathbf{U}$ follows from (23)

$$\mathbf{U} = \begin{Vmatrix} \frac{1}{s_{i+1j}(1-v_1)} & 0 & 0 \\ 0 & \frac{1}{s_{ij}+s_{i+1j}v_1+s_{ij-1}v_2} & 0 \\ 0 & 0 & \frac{1}{s_{ij-1}(1-v_2)} \end{Vmatrix}.$$

Now we can calculate

$$\widehat{\mathbf{M}}_{\mu^{-1}} = \frac{1}{\mu} \begin{Vmatrix} \frac{1}{s_{i+1j}}\left(1 + v_1\left(\frac{v_1 s_{i+1j}}{S_{\text{USC}}} - 1\right)\right) & \frac{1}{S_{\text{USC}}} v_1 & \frac{1}{S_{\text{USC}}} v_1 v_2 \\ \frac{1}{S_{\text{USC}}} v_1 & \frac{1}{S_{\text{USC}}} & \frac{1}{S_{\text{USC}}} v_2 \\ \frac{1}{S_{\text{USC}}} v_1 v_2 & \frac{1}{S_{\text{USC}}} v_2 & \frac{1}{s_{ij-1}}\left(1 + v_2\left(\frac{v_2 s_{ij-1}}{S_{\text{USC}}} - 1\right)\right) \end{Vmatrix}, \tag{A.2}$$

where

$$S_{\text{USC}} = s_{ij} + v_1 s_{i+1j} + v_2 s_{ij-1}.$$

From the comparison of (A.1) and (A.2) we conclude that with

$$\frac{S_1}{s_{i+1j}} = v_1, \quad \frac{S_2}{s_{ij-1}} = v_2,$$

or

$$v_1^0 = \frac{S_1}{s_{i+1j} - S_1}, \quad v_2^0 = \frac{S_2}{s_{ij-1} - S_2}$$

the ECT and USC schemes coincide.

References

[1] K.S. Yee, Numerical solution of initial boundary value problems involving Maxwell's equations in isotropic media, IEEE Trans. Antennas Propagat. 14 (1966) 302.
[2] R. Holland, Pitfalls of staircase meshing, IEEE Trans. Electromagn. Compat. 35 (1993) 434.
[3] A.C. Cangellaris, D.B. Wright, Analysis of the numerical error caused by the stair-stepped approximation of a conducting boundary in FDTD simulations of electromagnetic phenomena, IEEE Trans. Antennas Propagat. 39 (1991) 1518.
[4] T.G. Jurgens, A. Taflove, K. Umashankar, T.G. Moore, Finite-difference time-domain modelling of curved surfaces, IEEE Trans. Antennas Propaga. (1992) 357.
[5] C.J. Railton, I.J. Craddock, J.B. Schneider, Improved locally distorted CPFDTD algorithm with provable stability, Electron. Lett. 31 (1995) 1585.

[6] S. Dey, R. Mittra, A locally conformal Finite-Difference Time-Domain(FDTD) algorithm for modeling three-dimensional perfectly conducting objects, IEEE Microwave Guided Wave Lett. 7 (1997) 273.
[7] P. Thoma P, Zur numerischen Lösung der Maxwellschen Gleichungen im Zeitbereich, Ph.D. dissertation, D17, TH Darmstadt, Germany, 1997.
[8] R. Holland, V.P. Cable, L.C. Wilson, Finite-Volume Time-Domain (FVTD) techniques for EM scattering, IEEE Trans. Electromagn. Compa. 33 (1991) 281.
[9] R. Schuhmann, Die Nichtorthogonale Finite-Integrations-Methode zur Simulation elektromagnetischer Felder, Ph.D. dissertation, D17, TH Darmstadt, Germany, 1997.
[10] K.S. Yee, J.S. Chen, The finite-difference time-domain (FDTD) and the finite-volume time-domain (FVTD) methods in solving Maxwell's equations, IEEE Trans. Antennas Propagat. 45 (1997) 354.
[11] Y. Hao, C. Railton, Analyzing electromagnetic structures with curved boundaries on Cartesian FDTD meshes, IEEE Trans. Microwave Theory Tech. 46 (1998) 82.
[12] W. Yu, R. Mittra, A conformal FDTD software package modeling antennas and microstrip circuit components, IEEE Antennas Propagat. Mag. 42 (2000) 28.
[13] M. Yang, R. Mittra, Hybrid finite-difference/finite-volume time-domain analysis for microwave integrated circuits with curved PEC surfaces using a nonuniform rectangular grid, IEEE Trans. Microwave Theory Tech. 48 (2000) 969.
[14] A. Ditkowski, K. Dridi, J.S. Hesthaven, Convergent Cartesian grid methods for Maxwell's equations in complex geometries, J. Comput. Phys. 170 (2001) 39.
[15] F. Collino, P. Joly, F. Millot, Fictious domain method for unsteady problems: application to electromagnetic scattering, J. Comput. Phys. 138 (1997) 907.
[16] I.A. Zagorodnov, R. Schuhmann, T. Weiland, A uniformly stable conformal FDTD-method in Cartesian grids, Int. J. Numer. Model: Electron. Networks, Dev. Fields 16 (2003) 127.
[17] T. Weiland, A discretization method for the solution of Maxwell's equations for six-component fields, Electron. Commun. (AEÜ) 31 (1977) 16.
[18] T. Weiland, On the numerical solution of Maxwell's equations and applications in the field of accelerator physics, Particle Accelerators 15 (1984) 245.
[19] T. Weiland, On the unique solution of Maxwellian eigenvalue problems in three dimensions, Particle Accelerators 17 (1985) 227.
[20] T. Weiland, Time domain electromagnetic field computation with finite difference methods, Int. J. Numer. Model.: Electron. Networks, Dev. Fields 9 (1996) 295.
[21] T. Weiland, R. Schuhmann, Space and time stability of discrete time domain algorithm, in: Proceedings of the Fourth International Workshop on Computational Electromagnetics in the Time Domain (CEM-TD), Nottingham, UK, 2001, pp. 155–161.
[22] R.A. Horn, C.R. Johnson, Matrix Analysis, Cambridge University Press, Cambridge, 1986.
[23] F. Edelvik, R. Schuhmann, T. Weiland, A general stability analysis of FIT/FDTD applied to lossy dielectrics and lumped elements, Int. J. Numer. Model.: Electron. Networks, Dev. Fields 17 (2004) 407.
[24] T. Xiao, Q.H. Liu, Enlarged cells for the conformal FDTD method to avoid the time step reduction, IEEE Microwave and Wireless Components Letter 14 (2004) 553.
[25] K. Simonyi, Foundations of Electrical Engineering, Pergamon Press, London, 1963.
[26] I. Zagorodnov, R. Schuhmann, T. Weiland, Long-time computation of electromagnetic fields in the vicinity of a relativistic source, J. Comput. Phys. 191 (2003) 191.
[27] I. Zagorodnov, T. Weiland, TE/TM scheme for computation of electromagnetic fields in accelerators, J. Comput. Phys. 207 (2005) 69.
[28] R. Schuhmann, I. Zagorodnov, T. Weiland, Comment on ''Enlarged cells for the conformal FDTD method to avoid the time step reduction'', IEEE Microwave and Wireless Components Letter 16 (2006) 55.
[29] T. Xiao, Q.H. Liu, Reply to 'Comment on ''Enlarged cells for the conformal FDTD method to avoid the time step Reduction''', IEEE Microwave and Wireless Components Letter 16 (2006) 55.
[30] M. Woods, et al., A test facility for the international linear collider at SLAC end station A, SLAC-PUB-11180, 2005.